Molecular Dynamics Investigation of Cl^- and Water Transport through a Eukaryotic CLC Transporter

Mary Hongying Cheng and Rob D. Coalson*
Department of Chemistry, University of Pittsburgh, Pittsburgh, Pennsylvania

ABSTRACT Early crystal structures of prokaryotic CLC proteins identified three Cl^- binding sites: internal (S_{int}), central (S_{cen}), and external (S_{ext}). A conserved external GLU (GLU_{ex}) residue acts as a gate competing for S_{ext}. Recently, the first crystal structure of a eukaryotic transporter, CmCLC, revealed that in this transporter GLU_{ex} competes instead for S_{cen}. Here, we use molecular dynamics simulations to investigate Cl^- transport through CmCLC. The gating and Cl^-/H^+ transport cycle are inferred through comparative molecular dynamics simulations with protonated and deprotonated GLU_{ex} in the presence/absence of external potentials. Adaptive biasing force calculations are employed to estimate the potential of mean force profiles associated with transport of a Cl^- ion from S_{ext} to S_{int}, depending on the Cl^- occupancy of other sites. Our simulations demonstrate that protonation of GLU_{ex} is essential for Cl^- transport from S_{ext} to S_{cen}. The S_{cen} site may be occupied by two Cl^- ions simultaneously due to a high energy barrier (~8 Kcal/mol) for a single Cl^- ion to translocate from S_{cen} to S_{int}. Binding two Cl^- ions to S_{cen} induces a continuous water wire from S_{cen} to the extracellular solution through the side chain of the GLU_{ex} gate. This may initiate deprotonation of GLU_{ex}, which then drives the two Cl^- ions out of S_{cen} toward the intracellular side via two putative Cl^- transport paths. Finally, a conformational cycle is proposed that would account for the exchange stoichiometry.

INTRODUCTION

The CLC membrane protein family consists of nine members in mammalian species, which play critical roles in regulating the membrane action potential, muscle excitability (CLC-1), renal intravascular transport (CLC-K and CLC-5), and cell flexibility (CLC-2 and CLC-3) (1–4). The CLC superfamily includes both prokaryotic and eukaryotic members. It is composed of two subclasses: channels for selective permeation of Cl^- ions and transporters for exchange of two Cl^- ions in one direction with one proton in the opposite direction (5–7). Despite fundamental differences in functionality, members of the CLC family of channel/transporter protein are believed to share structural similarity (3,8,9) and its channel members are now thought to be evolutionally degraded transporters (3). The CLC protein is a dimer that adopts a double-barreled configuration in the transmembrane (TM) domain (8,10). Each subunit comprises an independent ion transport pore (11) regulated by a fast gate (3). The eukaryotic family members possess an additional cytosolic cystathionine β-synthase domain on the intracellular side (3,12).

Early x-ray crystallization of prokaryotic EcCLC and StCLC transporters (8,10) identified a narrow 15 Å selectivity filter region inside the transporters with two anion-binding sites: one near the intracellular entrance to the selectivity filter (S_{int}), and the other in the center of the filter (S_{cen}). The putative gating glutamate residue (GLU_{ex}; E148 in EcCLC) occupied the third anion binding site (S_{ext}) near the extracellular entrance to the selectivity filter. Recently, the first x-ray crystal structure of a eukaryotic CLC transporter from the thermophilic red alga *Cyanidioschyzon merolae* (CmCLC) revealed that the homologous GLU_{ex} gate (E210 in CmCLC) occupied the S_{cen} site instead of S_{ext} (12). How this conformation relates to the Cl^- transport cycle remains elusive due to the lack of a complete set of intermediate conformation states (12). In the CmCLC transport cycle model provided by MacKinnon's group (12), one major assumption is the existence of a high energy barrier that prevents a rapid movement of Cl^- ions from S_{cen} to S_{int}.

Two (8,10,12) and three (13) anion binding sites identified in the x-ray crystal structures point to the existence of a curved Cl^- ion transport route connecting the intracellular and extracellular solutions. The GLU_{ex} gate, together with a central gate formed by a conserved SER residue (S107 in EcCLC and S165 in CmCLC) and TYR residue (Y445 in EcCLC and Y515 in CmCLC), are proposed to coordinate the transport of Cl^- (1,3). Whereas Cl^- binding to S_{cen} is suggested to be essential for coupled proton translocation (14,15) in EcCLC, in the newly resolved CmCLC crystal structure (12), the GLU_{ex} gate rather than Cl^- occupies S_{cen}. This finding raises the possibility that occupancy of S_{cen} by the GLU_{ex} gate residue in CmCLC may play a similar role as found for a Cl^- ion at the S_{cen} site in EcCLC (14,15).

At present, the proton transport pathway through CLC transporters is largely unknown because crystallographic resolution is not high enough to capture proton binding. It has been proposed that a common path is shared by protons and Cl^- for translocation from the extracellular solution to the GLU_{ex} gate, but that the two routes bifurcate from GLU_{ex} toward the intracellular solution for chloride versus proton transport (16). In the bacterial transporters, two

Submitted October 31, 2011, and accepted for publication January 24, 2012.

*Correspondence: coalson@pitt.edu

Editor: Jose Faraldo-Gomez.

© 2012 by the Biophysical Society

0006-3495/12/03/1363/9 $2.00

doi: 10.1016/j.bpj.2012.01.056

glutamate residues near the extracellular (E148 in EcCLC) and intracellular solution (E203 in EcCLC) are suggested as dual gates (GLU_{ex} and GLU_{in}) (3,16–19). Theoretical studies of the proton transport (20–22) broadly agree with experimental implications. Recent reactive molecular dynamics (MD) simulations (23) have shown that Cl^- binding to both S_{cen} and S_{int} sites is essential for proton transport from the GLU_{in} to GLU_{ex} gate in the bacterial EcCLC transporter.

Several types of CLC transporters exchange chloride ions with protons in a tight 2:1 stoichiometry (2,3,17,18). Currently, there is no definitive explanation how the Cl^- ion and proton motions are coupled. Transport cycle models for the CLC transporters have been proposed by Beck (22), Accardi (24), Maduke (25), Chen (26), and, recently, Miloshevsky and Jordan (27) and MacKinnon's group (12). These models have a common feature: the transport cycle of $2Cl^-/H^+$ is determined by alternately exposing substrate binding sites through appropriate protein conformation changes (25,27). Miller and Nguitragool (6) proposed a fundamentally different model, in which the exchange stoichiometry is resolved by simultaneous binding of two Cl^- and one proton at the S_{cen} site. However, this model requires the formation of HCl and the opening of the inner gate (GLU_{in}) twice per transport cycle (6).

Extant crystal structures have revealed several stable intermediate conformations. However, a complete understanding of the CLC transport cycle will require identification of several as yet undiscovered CLC conformation states (12). To complement experimental efforts, MD simulation (20,28,29) and coarse-grained modeling (21,22,27,30) have emerged as valuable tools for elucidating dynamical processes within CLC proteins. In this study, we employ MD to investigate the Cl^- transport cycle and exchange stoichiometry in CmCLC. Free energy calculations are performed to test the CmCLC transport cycle model provided by MacKinnon's group (12).

METHODS

MD simulations

Three missing loops (L295 to D314, F375 to P382, and V393 to T404) in the TM domain of the CmCLC crystal structure (PDB: 3ORG) (12) were reconstructed based on the bacterial EcCLC (PDB: 1OTS) (8) using MODELER 9.0 for homology modeling (31). The missing loop between V600 and V656 in the extracellular domain was not restored, but we restrained Cα of residues (I588 to V600, and V656 to V666) near this missing loop using harmonic restraints (1.0 $kcal\cdot mol^{-1}\cdot Å^{-2}$) during the MD simulations. Subsequently, the TM domain of the CmCLC was inserted into the center of a preequilibrated POPE/POPG (3:1) binary lipid mixture as used in the experimental study (12). Fully equilibrated TIP3 waters and 0.3 M KCl were added to the system to form an all-atom simulation system 100 Å × 135 Å × 106 Å in extent. The complete simulation system was composed of two subunits, 199 POPE molecules, 63 POPG molecules, and ~25,000 water molecules for a total of over 128,000 atoms. Fig. 1 illustrates the MD setup of the initial system.

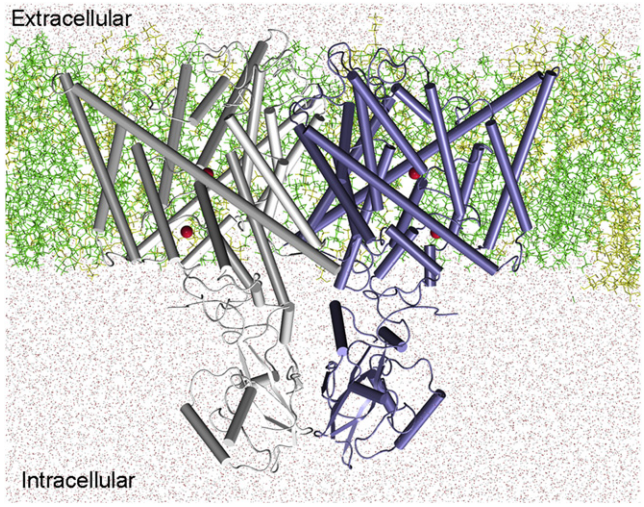

FIGURE 1 MD setup of CmCLC embedded into a POPE/POPG (3:1) binary membrane lipid bilayer and solvated by symmetric 0.3 M KCl bathing solutions (ions not shown). The two subunits in the CmCLC are colored differently. Spheres (*red*) depict four Cl^- ions found in the crystal structure. POPE and POPG lipid molecules, represented in line format (colored by *green* and *yellow*, respectively), constitute the bilayer membrane. Water is shown as dots. The channel axis z runs from the extracellular to intracellular side. (*Color online*.)

Two control simulation systems were generated using different protonation states of these two GLU_{ex} gates: 1), both GLU_{ex} residues were protonated (denoted as A_pB_p or System 1); 2), both GLU_{ex} residues were deprotonated (termed as A_dB_d or System 2). To explore the transport cycle for Cl^- ions, we assembled additional simulation systems (Systems 3 to 8) with different Cl^- occupancies and protonation states of GLU_{ex} gates. Moreover, a Y265A mutation was performed on both subunits of System 2 to further investigate the putative proton transport path. The essential characteristics of each system are summarized in Table 1 and illustrated in Fig. S1 in the Supporting Material.

Simulations were carried out using NAMD (32) following standard MD procedure. The CHARMM27 force field with CMAP corrections (version 31) was used for protein, water, and lipids (33). For Systems 1 and 2, the system was first energy minimized for 20,000 conjugate gradient steps and subsequently equilibrated for 2 ns, during which the backbone constraint on CmCLC was gradually reduced from 10 $kcal\cdot mol^{-1}\cdot Å^{-2}$ to zero. These two control systems were subjected to unrestrained Nosé-Hoover constant pressure (P = 1 Bar) and temperature (T = 310 K) (NPT) (34,35) simulations for 80 ns, which were then continued for another 20 ns under an applied electric field (36) of −0.1 Kcal/(mol Å e) along the transmembrane direction (z axis). This applied external potential, corresponding to a −120 mV transmembrane potential (assuming the membrane thickness is ~30 Å), drove a Cl^- ion from the extracellular side to the intracellular side. Mutated CmCLC simulations were subjected to the same procedure as System 2 and were simulated for up to 14 ns. Systems 3 to 8 were energy minimized for 5,000 steps, followed by 300 ps of equilibration, during which the backbone constraint was gradually released. Subsequently, unrestrained NPT simulation was performed under the same external electric field as in the control systems. A detailed simulation protocol is provided in the Supporting Material.

PMF calculations

The single ion potential of mean force (PMF) profiles for transporting a Cl^- ion from S_{ext} to S_{cen} and S_{int} were calculated along the transport path using

TABLE 1 Summary of simulation systems

System	Protonation state of E210	Occupied Cl^- sites	Initial protein structure	Simulation length (ns)	External potential Kcal/(mol Å e)
1 (A_PB_P)	Protonated A B	S_{ext} and S_{int}	X-ray	100	After 80 ns, −0.1
2 (A_dB_d)	Deprotonated A B	S_{ext} and S_{int}	X-ray	100	After 80 ns, −0.1
3	Deprotonated A B	S_{cen}	84 ns of A_pB_p	8	−0.1
4	A_dB_p*	S_{ext} and S_{int}	80 ns of A_pB_p	50	−0.1
5	A_dB_p*	S_{cen} and S_{ext}	Snapshot from 4‡	20	−0.1
6	A_dB_p*	S_{int} S_{cen} and S_{ext}	Snapshot from 4‡	40	−0.1
7	Deprotonated A B	S_{cen}	Snapshot from 5	40	−0.1
8	Deprotonated A B	S_{cen}	Snapshot from 5	30	−0.1
Y265A	Deprotonated A B	S_{ext} and S_{int}	X-ray	14 ns	0.0

*Deprotonated E210 in subunit A and protonated E210 in subunit B.
‡Cl^- ion at S_{ext} was docked manually.

the adaptive biasing force (37,38) method implemented in NAMD (32). Energy barriers for Cl^- transport were estimated based on the PMF profiles. Detailed adaptive biasing force calculations are presented in the Supporting Material. The GLU_{ex} gate E210 is characterized by two dihedral angles, $\chi1$ (defined by N CA CB and CG atoms) and $\chi2$ (defined by CA CB CG and CD atoms); cf. Fig. S2 *A*. A two-dimensional (2D) dihedral PMF was calculated for both the protonated (A_pB_p system) and deprotonated (A_dB_d system) E210 residues using Metadynamics as implemented in NAMD (32). The height and width of the Gaussian potentials employed in these calculations are 0.01 and $\sqrt{2\pi}/2$, respectively. The time interval between Gaussian functions is 0.2 ps. For each system, a total of 16 ns MD simulations were carried out, during which one Cl^- ion remained bound to the S_{ext} site identified in the crystal structure (PDB:3ORG). The standard deviations for the PMF calculations were estimated from different runs on different subunits and also from MD simulations of different lengths.

RESULTS AND DISCUSSION

Structural stability and variability

The overall stability of CmCLC structures (in the A_dB_d and A_pB_p systems) was evaluated using the root mean-square deviation (RMSD) of backbone Cα atoms away from the initial configurations. The two protein structures, with either protonated or deprotonated GLU_{ex} gate (E210), displayed a stabilized RMSD after ~10 ns MD simulations, with the steady-state RMSD from the initial configuration being ~2.7 ± 0.3 Å. The most significant deviation resulted from the reconstructed loops that were missing from the crystal structure: the RMSD was reduced to 2.0 ± 0.2 Å when these missing loops were omitted from the calculations.

In the initial x-ray structure, two hydrogen bonds between the two oxygen atoms from the carboxyl group of E210 were formed, with the hydroxyl groups of S165 and Y515 (12). These two hydrogen bonds assisted the binding of the GLU_{ex} gate to the S_{cen} site. During the simulations, the two hydrogen bonds eventually broke, thereby inducing conformational changes of the S_{ext} and S_{cen} sites. Fig. 2 compares the MD-relaxed structures with the corresponding initial configurations under different protonation states of the GLU_{ex} gate. Protonating the GLU_{ex} gate (E210) generated a local reorganization of the side-chain orientation of E210 or the nearby Y265 residue (not shown) and no significant secondary structural changes were observed due to protonation.

Protonation of the GLU_{ex} gate facilitates Cl^- transport from S_{ext} to S_{cen}

The side-chain orientation of the GLU_{ex} gate is characterized by its dihedral angles $\chi1$ and $\chi2$. Only two sets of dihedral angles were observed for a deprotonated GLU_{ex} gate in our simulations of the A_dB_d system, one in each of the two subunits: $\chi1 = 50 \pm 20°$ and $\chi2 = 80 \pm 20°$, and $\chi1 = 80 \pm 20°$ and $\chi2 = -65 \pm 20°$ (Fig. 3, *B* and *A*,

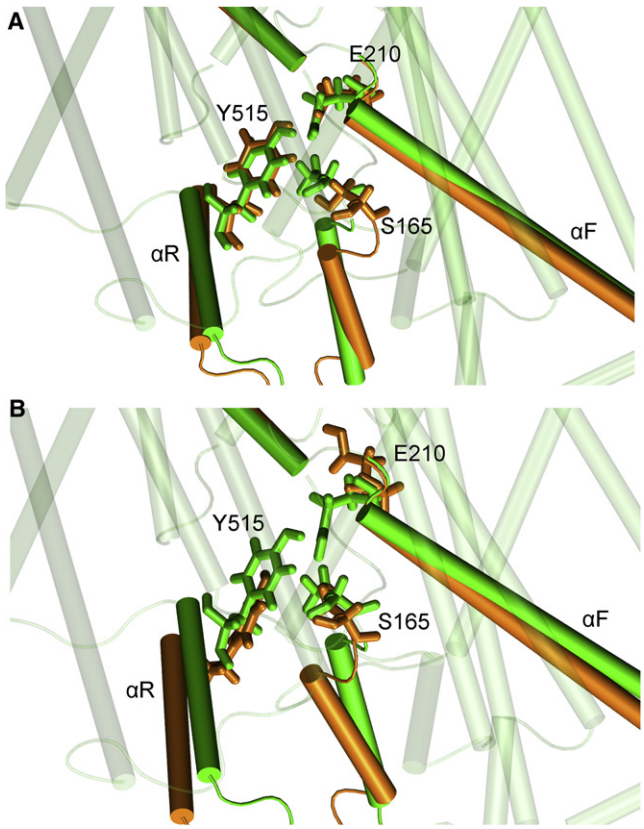

FIGURE 2 Alignment of initial configuration (colored in *white*) (*green* in the online figure) with MD equilibrated structure (colored in *dark gray*) (*orange* in the online figure) in the: (*A*) A_dB_d system and (*B*) A_pB_p system. Extracellular region is at top of plot, and intracellular region is at the bottom. (*Color online*.)

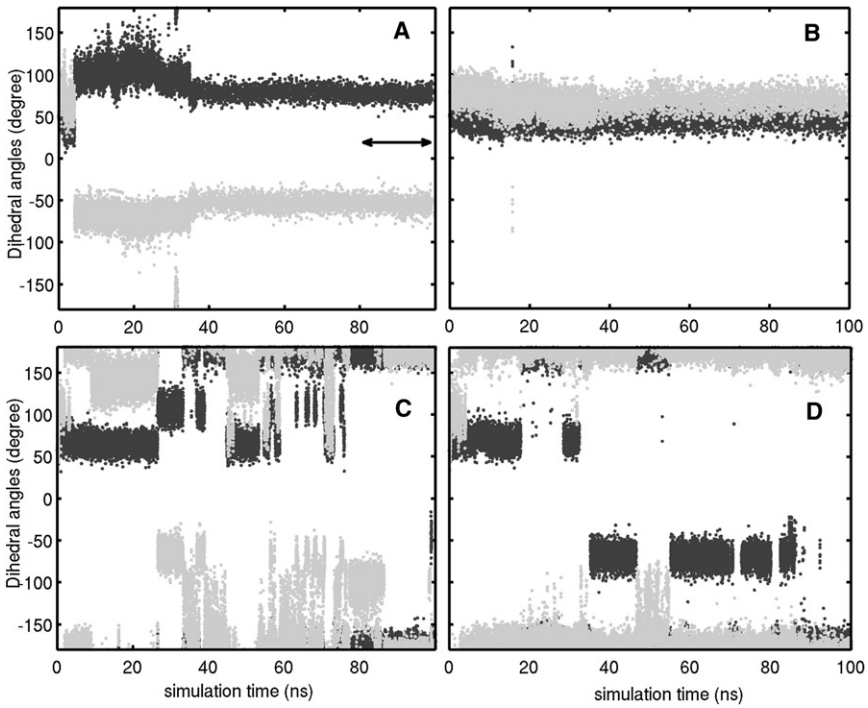

FIGURE 3 Time evolution of dihedral angles $\chi 1$ (*black*) and $\chi 2$ (*gray*) in (*A*) subunit A and (*B*) subunit B of the A_dB_d system; and in (*C*) subunit A and (*D*) subunit B of the A_pB_p system. Top and bottom panels show simulations with deprotonated and protonated E210, respectively. In both systems, an external potential was applied after 80 ns NPT simulations, as demarcated by the double-arrow line in panel *A*. Typical orientations of E210 in the different systems are shown in Fig S2 of the Supporting Material.

respectively). These two dihedral orientations were also observed in Systems 3 to 8 for the deprotonated GLU_{ex} gate, as indicated by the two minima appearing in the 2D dihedral PMFs (shown in *dark blue* in Fig. 4 *A*). The first set of dihedral angles corresponds roughly to the GLU_{ex} orientation found in the x-ray structure. In this orientation, the Cl^- ion initially located at the S_{ext} site remained there during the entire simulation (Fig. S3). When the GLU_{ex} gate reoriented to the second set of dihedral angles, the binding of the Cl^- ion to the S_{ext} site became unstable and Cl^- ultimately left the S_{ext} site toward the extracellular solution without any applied potential. For the deprotonated E210, the calculated energy barrier is $>30 \pm 5$ Kcal/mol for Cl^- to transport from S_{ext} to S_{cen} in both subunits, with a slightly lower value for the orientation suggested by the crystal structure. Such a high energy barrier completely prevents Cl^- translocation from S_{ext} to S_{cen}.

Once the GLU_{ex} gate was protonated (A_pB_p system), its dihedral angles $\chi 1$ and $\chi 2$ significantly deviated from their original values in the crystal structure. The free energy increase for a protonated GLU_{ex} gate to adopt the orientation identified in the crystal structure is ~5.6 $\pm$ 1.0 Kcal/mol, as compared to the most favorable orientations for a protonated GLU_{ex} gate (Fig. 4 *B*). This suggests that the GLU_{ex} gate in the x-ray structure may be deprotonated. As shown in Fig. 3, *C* and *D*, $\chi 1$ and $\chi 2$ of the protonated GLU_{ex} gate displayed a much broader range of values than those found for a deprotonated GLU_{ex}, varying between 50 $\pm$ 20° and 180° or $-50 \pm 20°$ and $-180°$. Such a large variation of dihedral orientation is consistent with our 2D dihedral PMFs for the

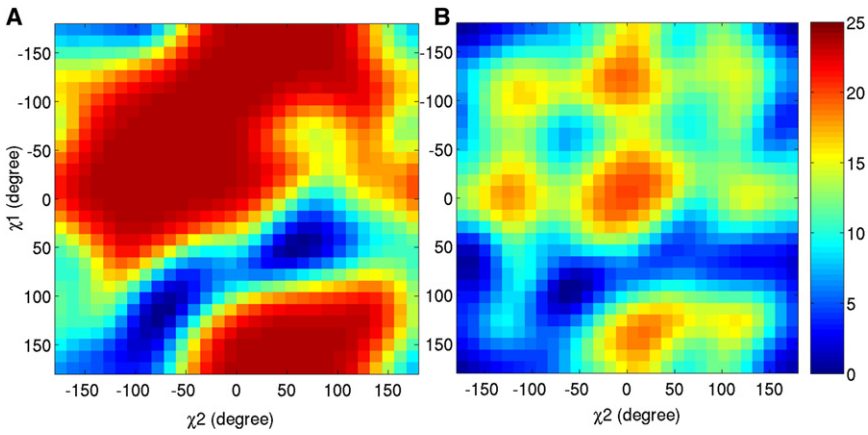

FIGURE 4 2D dihedral PMFs with (*A*) deprotonated E210 in the A_dB_d system and (*B*) protonated E210 in the A_pB_p system. PMFs are given in Kcal/mol (see scale bar at *right*). (*Color online*.)

protonated E210 (Fig. 4 *B*). Under an applied external transmembrane potential of −120 mV, within 4 ns the dihedral angles in both protonated GLU_{ex} gates quickly evolved to become $\chi1 = 180°$ (or −180°) and $\chi2 = 180°$ (or −180°) and remained at these values as Cl^- transported from S_{ext} to S_{cen}. Simultaneously, a continuous water path was formed from the extracellular solution to the S_{ext} site (Fig. S4). For the protonated GLU_{ex} gate, the calculated energy barrier for Cl^- transport from S_{ext} to S_{cen} was around 2.5 ± 1.0 Kcal/mol (cf. Fig. 5), which is significantly reduced in comparison to the deprotonated GLU_{ex}. Protonation of GLU_{ex} opened the gate for Cl^- transport (Fig. S5). During 80 ns of the MD simulation without any applied external potential, the side chain of the protonated GLU_{ex} gate swung away from the S_{cen} site and gradually rotated toward the S_{ext} site (Fig. S5), consistent with the CmCLC transport model (12) proposed by Mackinnon's group.

Putative proton transport path inferred from continuous water path

In both subunits of the A_pB_p system with protonated GLU_{ex} gates, the αF helix underwent a 5° clockwise rotation toward the intracellular domain and the helix αR (containing Y515) moved (or rotated) toward the intracellular domain (Fig. 2). The motion of the αR helix together with a local reorganization of residues near GLU_{ex} induced a stable continuous water wire starting from the intracellular solution and extending to the GLU_{ex} gate (Fig. S4).

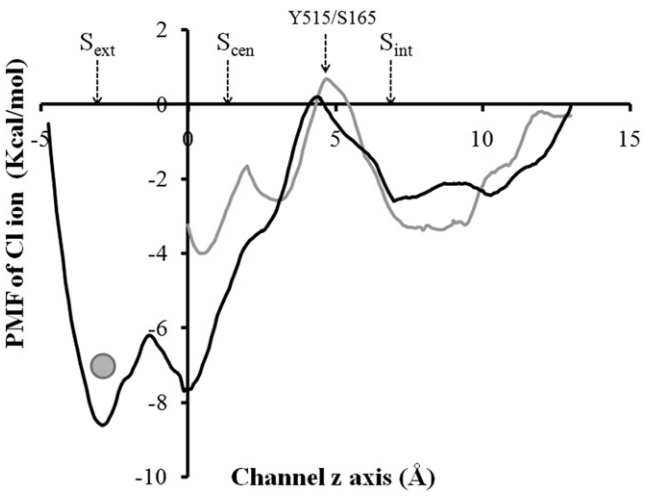

FIGURE 5 Potentials of mean force for Cl^- transport from the S_{ext} site to the intracellular solution in the protonated GLU_{ex} system (A_pB_p system). The single ion PMF is shown via a black line. Gray line represents the PMF for transport of one Cl^- ion from S_{cen} to intracellular solution with another Cl^- bound to the S_{ext} site. The position of the bound Cl^- is indicated by a solid circle in the figure. In the PMF calculations, the bound Cl^- ion is restrained using an isotropic three-dimensional harmonic restraint (with force constant of 1.0 $kcal \cdot mol^{-1} \cdot Å^{-2}$) at the external binding site S_{ext} suggested by the crystal structure (PDB: 3ORG).

This continuous water path has been proposed as the proton transport pathway in the bacterial CLC transporters (20–22). Previously, the GLU_{in} gate was suggested to be strictly conserved in CLC transporters but to be substituted by a hydrophobic residue VAL in all-known CLC channels (16). Neutralization of the GLU_{in} gate was found to abolish coupled proton and Cl^- transport (16) in EcCLC as well as in CLC-4 and CLC-5 (39). The CmCLC transporter does not possess a GLU_{in} gate. Instead, a hydrophilic THR residue (T269) occupies the homologous position. This THR residue was found to line the water pore observed in our MD simulations. Feng et al. (12) proposed that this THR residue may play the role of the GLU_{in} gate for proton transport. However, the question has been raised as to the ability of THR to act as a proton donor (21). Hence, we examined other residues in CmCLC along this putative proton transport pathway. In addition to E210, T269, and Y515 residues, whose homologous residues have previously been found to be important for proton transport in the bacterial CLC transporter (14,16), Y265 appears to be a good candidate to further test its role in the proton transport process based on our MD simulations. Aromatic Y265 is conserved in the eukaryotic CLC family (see Fig. S1 of (12)) and lines the extracellular pore entrance of this putative proton transport path (Fig. S4). During a 100-ns MD simulation of the A_dB_d system (Fig. S6 *A*), a close interaction between Y265 and Y515 (i.e., hydrogen bonding) constricted this pathway and prevented the formation of a continuous water wire leading from the intracellular solution to the GLU_{ex} gate. Motion of helix αR toward the intracellular domain (as shown in Fig. 2 *B*) resulted in the breakage of several hydrogen bonds (such as those between Y515 and Y265 or Y515 and E210) and contributed to the formation of such a continuous water path for a deprotonated GLU_{ex} gate. In particular, in Systems 3 to 8 (where one GLU_{ex} gate was deprotonated after a simulation of 80 ns in the A_pB_p system), we observed that an initially continuous water path remained intact over the entire simulation interval (over 50 ns), running from either K171 or T269 to the deprotonated GLU_{ex} gate (Fig. S6 *B*). Interestingly, a Y265A mutation performed on the A_dB_d system was found to induce this putative proton transport water path within ~10 ns (Fig. S6 *C*). We thus suggest that a Y265A mutation may affect proton transfer due to its influence on the constriction of the putative proton transport path identified here.

Cl^- transport from S_{cen} to the intracellular solution

With a protonated GLU_{ex} gate (i.e., in the A_pB_p system), the calculated free energy barrier for a Cl^- ion to transport from S_{cen} to S_{int} was ~8.0 ± 2.5 Kcal/mol (Fig. 5). Such a large energy barrier would prevent rapid Cl^- translocation from S_{cen} to S_{int}, thus directly supporting the major hypothesis for the CmCLC transport cycle proposed by the Mackinnon

group (12). It should be noted that in motions of Cl^- ions that involve simultaneous large changes in the configuration of intrapore water molecules, the Cl^- coordinate itself may not represent an optimal reaction coordinate. However, because we are using these PMFs simply as a qualitative guide to possible steps in the transport mechanism of CmCLC (not for the quantitative prediction of equilibrium constants or rate constants), the treatment we have given here should suffice.

In the PMF calculations, the side chains of S165 and Y515 constricted the Cl^- permeation path and impeded a partially dehydrated Cl^- ion from transporting between S_{cen} and S_{int} (Fig. 5 and Fig. S7). Thus, S165 and Y515 in the CmCLC may function as a second gate for Cl^- permeation, as found for their bacterial homologous residues in EcCLC (1,3,6). Overcoming the energy barrier imposed by S165 and Y515 may in principle be initiated or facilitated by i), deprotonation of E210 or ii), by the arrival of another Cl^- ion from the extracellular solution. We performed several sets of MD simulations (System 3 to 8) to further test these two hypotheses.

Deprotonating E210

In System 3 (Fig. S1 *A*), we deprotonated the GLU_{ex} gates in a protein structure taken from the A_pB_p system, where the Cl^- ion originally at the S_{ext} site in the x-ray structure had already transported to the S_{cen} site in both subunits under an externally applied transmembrane potential of −120 mV. With a protonated GLU_{ex} gate, no Cl^- ion was observed to transport from S_{cen} to S_{int} in 20 ns of MD simulation. Upon deprotonation, the dihedral angles $\chi1$ and $\chi2$ of the GLU_{ex} gate evolved from identical 180° ± 20° (or −180° ± 20°) at the beginning (favorable orientation for a protonated GLU_{ex}) to become 80° ± 20° and −65° ± 15° (favorable orientation for a deprotonated GLU_{ex}), respectively (Fig. S8). As soon as the GLU_{ex} gate altered its orientation, the Cl^- ion at the S_{cen} site was observed to quickly translocate to S_{int} within 6 ns of MD simulation. This transport is facilitated both by repulsive electrostatic interactions and by the orientation change of the GLU_{ex} side chain.

By protonating (A_pB_p system) and subsequently deprotonating (System 3) the GLU_{ex} gate, Cl^- ions located at S_{ext} and S_{int} in the x-ray crystal structure were observed to depart from their original binding sites and eventually transport to the intracellular solution in our simulations. This appears to result in translocation of two Cl^- ions in one transport cycle. However, there is one difficulty explaining the exchange stoichiometry of two Cl^- ions for one H^+ via this transport cycle. Namely, the motion of a Cl^- ion occupying the S_{int} site was not strongly correlated with the transport of Cl^- at the S_{ext} (or S_{cen}) site to the intracellular reservoir. Because the S_{int} site is exposed to the intracellular solution directly, it is easy for Cl^- at S_{int} to move in and out of S_{int} (see Fig. S3), thus producing motion that is uncoupled from that of Cl^- at S_{ext} (or S_{cen}), and resulting in a Cl^- transport cycle that loses tight stoichiometric coupling.

Two Cl^- ions competing for the S_{cen} site

For the bacterial CLC transporters, Miller and Nguitragool (6) proposed that an exchange stoichiometry of $2Cl^-/H^+$ requires binding of two Cl^- ions to the S_{cen} site. To test this hypothesis in the context of CmCLC, we designed several numerical simulations. In one system (System 5; see Fig S1 *C*), two Cl^- ions were bound simultaneously to S_{ext} and S_{cen} in one subunit having a protonated GLU_{ex} gate. Binding of Cl^- ions simultaneously to S_{ext} and S_{cen} has been observed in the crystal structure of E148A of the bacterial EcCLC transporter (13). Recent isothermal titration calorimetry measurement has also found that binding of two Cl^- ions to the E148A mutant (EcCLC) at S_{ext} and S_{cen} shows 10- to 60-fold higher affinity than to the isolated sites (1,40), thus supporting our initial configuration of binding two Cl^- ions to S_{ext} and S_{cen} (one at each site), because E148A is considered as a mimic of the protonated GLU_{ex} gate (1). The binding of Cl^- to the S_{ext} site reduced the energy barrier for a Cl^- ion to transport from S_{cen} to S_{int} by 4.0 ± 1.5 Kcal/mol (Fig. 5). Such a reduction is in good agreement with a similar calculation performed on the bacterial StCLC transporter (41).

Under an externally applied potential of −120 mV, a Cl^- at S_{ext} was able to migrate within 10 ns to the S_{cen} site in the presence of another Cl^- already occupying the central binding site. These two Cl^- ions broadly exhibited two binding configurations (Fig. S9) within the S_{cen} site. One Cl^- ion bound near the backbone of the GLU_{ex} gate. The other Cl^- ion either resided close to the entrance of the previously proposed proton transport path (42,43) (Fig. S9 *A*; termed site A) or near the S_{int} site (Fig. S9 *B*; termed site B). Occupancy by two Cl^- ions of S_{cen} induced the formation of a continuous water wire from S_{cen} to the extracellular side through the side chain of GLU_{ex} (Fig. S9). The water path persisted as long as two Cl^- ions bound simultaneously to the S_{cen} site (life time > 10 ns). This continuous water wire may promote the dissociation of a proton from the protonated E210 residue, thus deprotonating GLU_{ex}.

To investigate how deprotonation of GLU_{ex} affects the transport of two Cl^- ions, we generated two independent simulation systems (System 7 and 8) using these two snapshots (Fig. S9, *A* and *B*) as the initial configurations (shown in Fig. S1, *E* and *F*) for MD investigation. Once the GLU_{ex} gate was deprotonated, in one system (System 7) the Cl^- ion at site A transported to the intracellular domain along the water path behind Y515 (*black arrow* in Fig. S9 *A*). In the other system (System 8), the Cl^- ion at site B moved to the S_{int} site (*black arrow* in Fig. S9 *B*) along the path elucidated by x-ray crystal structures. Finally, the remaining Cl^- ions took the same route (*black arrow* in Fig. S9 *B*) to S_{int} sites in both simulation systems within 40 ns.

Cl^- transport path(s)

As just noted, we observed two potential Cl^- transport paths from S_{cen} to the intracellular side (see Fig. S9). The Cl^- transport path shown in Fig. S9 *A* has been suggested in previous work to function as a proton transport path (22,43), but has not previously been implicated in Cl^- transport. We noticed that Cl^- had a higher probability to take this path when another Cl^- was bound to S_{ext} (such as state e and d of the CmCLC transport model from (12); probed in our System 6 simulations) or two Cl^- ions bound simultaneously to S_{cen} (the hypothesis employed in the Miller and Nguitragool model (6); probed in our System 7 simulations). With only one Cl^- bound to the S_{cen} site and no Cl^- ion bound to the S_{ext} site (System 3), deprotonation of the GLU_{ex} gate drove Cl^- exclusively along the path shown in Fig. S9 *B*.

Although it is premature to confidently predict the novel Cl^- transport route suggested above without explicitly considering coupled proton transport, it is worth testing in future experiments. Pore lining residues such as T269, K171, and Y265 were observed to coordinate the permeation of Cl^- through this new path, and thus mutations of these residues (such as T269E, K171L, and Y265A) may assist in assessing this pathway's role in Cl^- transport.

Cl^- transport cycle in the CmCLC

The Cl^- ions originally in S_{int} sites were observed under MD simulation to escape to the intracellular reservoir, and to be intermittently replaced by other Cl^- ions from the intracellular reservoir (Fig. S3). This process is thus assigned a negligible role in the transport cycle proposed here. To minimize the complexity of the state model, we only consider transport of one Cl^- initially at the S_{ext} site, similar to the strategy employed by Miller and Nguitragool (6). On the basis of our MD simulations, we propose a five-state Cl^- transport cycle (Fig. 6). The essential steps of the cycle are as follows:

A. Deprotonated GLU_{ex} gate (E210) blocks Cl^- transport from S_{ext} to S_{cen}.
B. Protonation of GLU_{ex} opens the gate for Cl^- to transport from S_{ext} to S_{cen}. A proton enters from the intracellular solution along a continuous water path formed behind Y515 (Fig. 6 *B*), which is presumably induced by the motion of helix αR toward the intracellular domain (as shown in Fig. 2 *B*). Upon protonation, the E210 residue moves away from the S_{cen} site.
C. One Cl^- ion moves in from the S_{ext} site via the backbone of the GLU_{ex} gate to occupy the S_{cen} site. A significant free energy barrier prevents this Cl^- ion from transporting to the intracellular reservoir.
D. A second Cl^- ion moves in from the extracellular reservoir to occupy the S_{cen} site. Occupancy by two Cl^- ions induces a continuous water wire from S_{cen} to the extracellular solution through the side chain of the GLU_{ex} gate.
E. The proton on E210 dissociates and exits to the extracellular solution. The resultant deprotonated E210 drives both Cl^- ions that are in the S_{cen} site to the intracellular solution. The E210 residue then swings back to the S_{cen} site and reorients as shown in state *A*. Another Cl^- ion moves to S_{ext} from the extracellular solution. The cycle thus returns to its initial state.

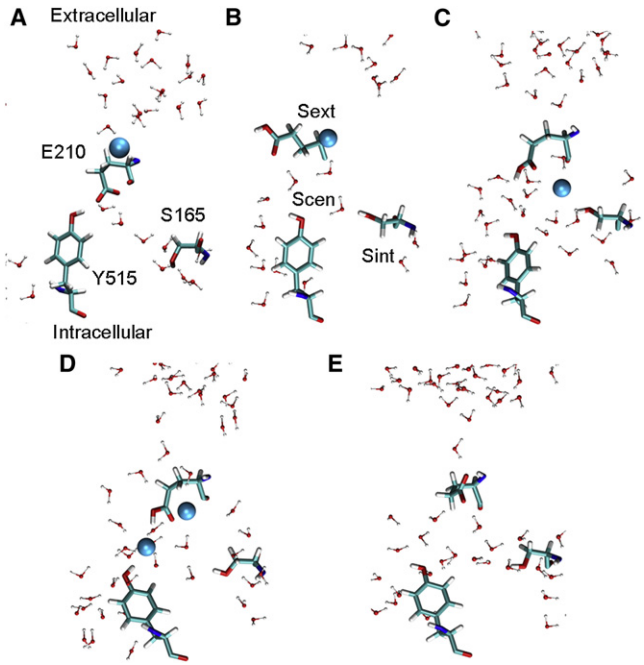

FIGURE 6 Schematic state diagram for Cl^- transport cycle in the CmCLC. (*A*) Deprotonated E210 blocks Cl^- translocation from S_{ext} to S_{cen}. (*B*) Protonation of E210 opens the GLU_{ex} gate. (*C*) One Cl^- ion transports to and occupies the S_{cen} site. (*D*) Two Cl^- ions reside in the S_{cen} site and a continuous water wire is formed from the S_{cen} site to the extracellular solution. (*E*) Deprotonation of the GLU_{ex} gate drives two Cl^- ions to the intracellular side. The cycle thus returns to its initial state *A*. Cl^- ions are shown as spheres (*cyan*). Each picture is taken from MD snapshots of different simulation systems. For simplification, only residues E210, Y515, and S165 are shown in licorice format and waters within 12 Å of E210 are shown in CPK format. Oxygen (*red*), nitrogen (*blue*), carbon (*cyan*), and hydrogen (*white*) atoms are colored differently. States *A* and *E* have deprotonated GLU_{ex} and states *B*, *C*, and *D* have protonated GLU_{ex}. (*Color online*.)

Note that the five-state transport model proposed herein does not require the formation of HCl and the opening of the inner gate (GLU_{in}) twice per transport cycle, as hypothesized in the EcCLC transport model by Miller and Nguitragool (6). In our model, we hypothesize that to maintain a strict $2Cl^-/H^+$ exchange ratio, the GLU_{ex} gate will only deprotonate when two Cl^- ions bind simultaneously to S_{cen}. As we observed in Systems 5 and 6, one Cl^- ion initially occupying S_{ext} transported to S_{cen} and resided in S_{cen} with another Cl^- ion already there. However, it should be noted that if the Cl^- originally occupied S_{cen} transports to

the intracellular solution before the permeation of a second Cl^- from S_{ext} to S_{cen}, the strict $2Cl^-/H^+$ exchange ratio will be broken. The degree of leakage via this mechanism depends on how easy it is for Cl^- at S_{ext} to transport to S_{cen} with a protonated GLU_{ex} gate (as explored in System 5), and how rapidly the GLU_{ex} deprotonates once a second Cl^- ion arrives at S_{cen}. Further analysis will be required to quantify the importance of this potential leakage mechanism with respect to the tight 2:1 antiport cycle process described above.

CONCLUSIONS

Using MD simulations, we have investigated the role of the GLU_{ex} gate for Cl^- transport in the CmCLC transporter. For the deprotonated GLU_{ex} gate, the calculated free energy barrier is $>30 \pm 5$ Kcal/mol for a Cl^- ion to transport from S_{ext} to S_{cen}, which is sufficiently high to prevent Cl^- transport. The opening of the GLU_{ex} gate involves the protonation of the GLU_{ex} gate and subsequent alteration of both dihedral angles to $\chi 1 = \pm 180°$ and $\chi 2 = \pm 180°$, which consequently reduces the energy barrier to a value of 2.5 ± 1.0 Kcal/mol for Cl^- to translocate from S_{ext} to S_{cen}. The S_{cen} site may be occupied by two Cl^- ions simultaneously due to a high free energy barrier (~8 Kcal/mol) for a single Cl^- ion to permeate from S_{cen} to S_{int}. Binding two ions to the S_{cen} site may be a crucial determinant of the $2Cl^-/H^+$ exchange stoichiometry: it can induce formation of a continuous water wire from S_{cen} to the extracellular solution. This may then initiate deprotonation of the GLU_{ex} gate, ultimately driving two Cl^- ions out of S_{cen} toward the intracellular side. Finally, we observed that Cl^- had a higher probability to transport through the previously-suggested proton transport path (20–22) than through the crystal-structure elucidated Cl^- conduction pathway when another Cl^- was bound to S_{ext} (such as state e and d of the CmCLC transport model from (12).), or two Cl^- ions bound simultaneously to S_{cen} (the hypothesis employed in the Miller and Nguitragool model (6)). To further evaluate this newly discovered Cl^- transport path and the coupled proton/Cl^- transport model proposed in this study, we suggest that experimental mutations be performed on residues Y265, T269, and K171 because these residues line a putative transport pathway for protons and/or Cl^- ions.

SUPPORTING MATERIAL

Additional Methods, Results and Discussion, nine figures, and reference (44) are available at http://www.biophysj.org/biophysj/supplemental/S0006-3495(12)00203-2.

We gratefully acknowledge financial support from the National Science Foundation (NSF) grant CHE-0750332 and computational support from the NSF through TeraGrid resources (TG-MCB100061 and TG-MCB110137). TeraGrid systems are hosted by Indiana University, Louisiana Optical Network Initiative (LONI), National Center for Atmospheric Research (NCAR), National Computational Science Alliance (NCSA), National Institute of Computational Sciences (NICS), Oak Ridge National Laboratory (ORNL), Pittsburgh Supercomputing Center (PSC), Purdue University, San Diego Supercomputer Center (SDSC), Texas Advanced Computer Center (TACC), and University of California/Argonne National Laboratory (UC/ANL).

REFERENCES

1. Accardi, A., and A. Picollo. 2010. CLC channels and transporters: proteins with borderline personalities. *Biochim. Biophys. Acta.* 1798:1457–1464.
2. Jentsch, T. J. 2008. CLC chloride channels and transporters: from genes to protein structure, pathology and physiology. *Crit. Rev. Biochem. Mol. Biol.* 43:3–36.
3. Miller, C. 2006. ClC chloride channels viewed through a transporter lens. *Nature.* 440:484–489.
4. Chen, T. Y. 2005. Structure and function of clc channels. *Annu. Rev. Physiol.* 67:809–839.
5. Picollo, A., M. Malvezzi, and A. Accardi. 2010. Proton block of the CLC-5 Cl^-/H^+ exchanger. *J. Gen. Physiol.* 135:653–659.
6. Miller, C., and W. Nguitragool. 2009. A provisional transport mechanism for a chloride channel-type Cl^-/H^+ exchanger. *Philos. Trans. R. Soc. Lond. B Biol. Sci.* 364:175–180.
7. Zifarelli, G., and M. Pusch. 2007. CLC chloride channels and transporters: a biophysical and physiological perspective. *Rev. Physiol. Biochem. Pharmacol.* 158:23–76.
8. Dutzler, R., E. B. Campbell, and R. MacKinnon. 2003. Gating the selectivity filter in ClC chloride channels. *Science.* 300:108–112.
9. Dutzler, R. 2007. A structural perspective on ClC channel and transporter function. *FEBS Lett.* 581:2839–2844.
10. Dutzler, R., E. B. Campbell, …, R. MacKinnon. 2002. X-ray structure of a ClC chloride channel at 3.0 A reveals the molecular basis of anion selectivity. *Nature.* 415:287–294.
11. Robertson, J. L., L. Kolmakova-Partensky, and C. Miller. 2010. Design, function and structure of a monomeric ClC transporter. *Nature.* 468:844–847.
12. Feng, L., E. B. Campbell, …, R. MacKinnon. 2010. Structure of a eukaryotic CLC transporter defines an intermediate state in the transport cycle. *Science.* 330:635–641.
13. Lobet, S., and R. Dutzler. 2006. Ion-binding properties of the ClC chloride selectivity filter. *EMBO J.* 25:24–33.
14. Accardi, A., S. Lobet, …, R. Dutzler. 2006. Synergism between halide binding and proton transport in a CLC-type exchanger. *J. Mol. Biol.* 362:691–699.
15. Nguitragool, W., and C. Miller. 2006. Uncoupling of a CLC Cl^-/H^+ exchange transporter by polyatomic anions. *J. Mol. Biol.* 362:682–690.
16. Accardi, A., M. Walden, …, C. Miller. 2005. Separate ion pathways in a Cl^-/H^+ exchanger. *J. Gen. Physiol.* 126:563–570.
17. Accardi, A., and C. Miller. 2004. Secondary active transport mediated by a prokaryotic homologue of ClC Cl^- channels. *Nature.* 427: 803–807.
18. Picollo, A., and M. Pusch. 2005. Chloride/proton antiporter activity of mammalian CLC proteins ClC-4 and ClC-5. *Nature.* 436:420–423.
19. Scheel, O., A. A. Zdebik, …, T. J. Jentsch. 2005. Voltage-dependent electrogenic chloride/proton exchange by endosomal CLC proteins. *Nature.* 436:424–427.
20. Wang, D., and G. A. Voth. 2009. Proton transport pathway in the ClC Cl^-/H^+ antiporter. *Biophys. J.* 97:121–131.
21. Kieseritzky, G., and E. W. Knapp. 2011. Charge transport in the ClC-type chloride-proton anti-porter from *Escherichia coli*. *J. Biol. Chem.* 286:2976–2986.

22. Kuang, Z. F., U. Mahankali, and T. L. Beck. 2007. Proton pathways and H+/Cl− stoichiometry in bacterial chloride transporters. *Proteins.* 68:26–33.

23. Zhang, Y., and G. A. Voth. 2011. The coupled proton transport in the ClC-ec1 $Cl^{(-)}/H^{(+)}$ antiporter. *Biophys. J.* 101:L47–L49.

24. Accardi, A. 2007. Structure and function of CLC chloride channels and transporters. *In* Chloride Movements Across Cellular Membranes. M. Pusch, editor. Elsevier, New York. 59–82.

25. Matulef, K., and M. Maduke. 2007. The CLC 'chloride channel' family: revelations from prokaryotes. *Mol. Membr. Biol.* 24:342–350.

26. Chen, T. Y., and T. C. Hwang. 2008. CLC-0 and CFTR: chloride channels evolved from transporters. *Physiol. Rev.* 88:351–387.

27. Miloshevsky, G. V., A. Hassanein, and P. C. Jordan. 2010. Antiport mechanism for $Cl^{(-)}/H^{(+)}$ in ClC-ec1 from normal-mode analysis. *Biophys. J.* 98:999–1008.

28. Bostick, D. L., and M. L. Berkowitz. 2004. Exterior site occupancy infers chloride-induced proton gating in a prokaryotic homolog of the ClC chloride channel. *Biophys. J.* 87:1686–1696.

29. Cohen, J., and K. Schulten. 2004. Mechanism of anionic conduction across ClC. *Biophys. J.* 86:836–845.

30. Faraldo-Gómez, J. D., and B. Roux. 2004. Electrostatics of ion stabilization in a ClC chloride channel homologue from *Escherichia coli*. *J. Mol. Biol.* 339:981–1000.

31. Šali, A., and T. L. Blundell. 1993. Comparative protein modelling by satisfaction of spatial restraints. *J. Mol. Biol.* 234:779–815.

32. Phillips, J. C., R. Braun, …, K. Schulten. 2005. Scalable molecular dynamics with NAMD. *J. Comput. Chem.* 26:1781–1802.

33. MacKerell, A. D., D. Bashford, …, M. Karplus. 1998. All-atom empirical potential for molecular modeling and dynamics studies of proteins. *J. Phys. Chem. B.* 102:3586–3616.

34. Nosé, S. 1984. A unified formulation of the constant-temperature molecular-dynamics methods. *J. Chem. Phys.* 81:511–519.

35. Hoover, W. G. 1985. Canonical dynamics: equilibrium phase-space distributions. *Phys. Rev. A.* 31:1695–1697.

36. Aksimentiev, A., and K. Schulten. 2005. Imaging alpha-hemolysin with molecular dynamics: ionic conductance, osmotic permeability, and the electrostatic potential map. *Biophys. J.* 88:3745–3761.

37. Darve, E., D. Rodríguez-Gómez, and A. Pohorille. 2008. Adaptive biasing force method for scalar and vector free energy calculations. *J. Chem. Phys.* 128:144120.

38. Chipot, C., and J. Hénin. 2005. Exploring the free-energy landscape of a short peptide using an average force. *J. Chem. Phys.* 123:244906.

39. Zdebik, A. A., G. Zifarelli, …, M. Pusch. 2008. Determinants of anion-proton coupling in mammalian endosomal CLC proteins. *J. Biol. Chem.* 283:4219–4227.

40. Picollo, A., M. Malvezzi, …, A. Accardi. 2009. Basis of substrate binding and conservation of selectivity in the CLC family of channels and transporters. *Nat. Struct. Mol. Biol.* 16:1294–1301.

41. Gervasio, F. L., M. Parrinello, …, M. L. Klein. 2006. Exploring the gating mechanism in the ClC chloride channel via metadynamics. *J. Mol. Biol.* 361:390–398.

42. Yin, J., Z. Kuang, …, T. L. Beck. 2004. Ion transit pathways and gating in ClC chloride channels. *Proteins.* 57:414–421.

43. Wang, X. Q., T. Yu, …, X. Zou. 2010. A three-state multi-ion kinetic model for conduction properties of ClC-0 chloride channel. *Biophys. J.* 99:464–471.

44. Darden, T., D. York, and L. Pedersen. 1993. Particle mesh Ewald - an N.Log(N) method for Ewald sums in large systems. *J. Chem. Phys.* 98:10089–10092.